Published in final edited form as:
Cell Calcium. 2015 January ; 57(1): 14–24. doi:10.1016/j.ceca.2014.11.002.

Role of Mitofusin-2 in Mitochondrial Localization and Calcium Uptake in Skeletal Muscle

Alina Ainbinder[1], **Simona Boncompagni**[2], **Feliciano Protasi**[2], and **Robert T. Dirksen**[1,*]

[1]University of Rochester School of Medicine and Dentistry, Department of Pharmacology and Physiology, Rochester, NY 14642

[2]CeSI - Centro Scienze dell'Invecchiamento & DNICS - Department of Neuroscience, Imaging and Clinical Sciences University G. d'Annunzio, I-66100 Chieti, Italy

1. Introduction

Being responsible for supporting body weight, maintaining posture, muscle thermogenesis, and producing explosive voluntary force and movement at a moment's notice, skeletal muscle is among the most metabolically active tissues in the body [1]. Almost 30% of all resting energy expenditure in humans involves skeletal muscle, and even more so, during exercise [2, 3]. ATP in skeletal muscle is produced primarily through either glycolysis (anaerobic) in the myoplasm or oxidative phosphorylation (aerobic) in mitochondria. However, the relative contribution of anaerobic versus aerobic energy production depends on muscle fiber type, as well as substrate availability and degree/form of activity.

Aerobic energy production in mitochondria depends highly on the mitochondrial functional state, which in turn, depends on the maintenance of a strong proton motive force (the sum of the inner mitochondrial membrane potential and pH gradient), appropriate intra-mitochondrial Ca^{2+} levels, and proper mitochondrial morphology. Mitochondrial morphology is maintained by a balance between fusion and fission [4]. Mitofusin (Mfn) is a transmembrane GTPase that participates in fusion of the mitochondrial outer membranes of two adjacent mitochondria [5]. Two Mfn isoforms (Mfn1 and Mfn2) are capable of forming homotypic and heterotypic complexes that bring the membranes of opposing mitochondria together to drive membrane fusion. Mfn1 is exclusively located in the mitochondrial outer membrane, while Mfn2 is found in both the outer mitochondrial membrane and the endoplasmic/sarcoplasmic (ER/SR) membrane [6, 7]. In non-excitable cells, mitochondria are connected to the ER membrane by ~10 nm electron dense bridges or "tethers". Tethers are composed of Mfn1 and Mfn2 proteins connected via an interaction mediated through their C termini [6]. By structurally attaching mitochondria to the ER, Mfn tethers mitochondria ~10 from the point source of ER Ca^{2+} release (via inositol 1,4,5-trisphosphate

*Corresponding Author:Robert_Dirksen@urmc.rochester.edu; Tel: +01-585-275-4824.

receptors), termed "Ca^{2+} release microdomains" where Ca^{2+} concentrations reach up to 10 times the global cytosolic concentration [8, 9]. This strategic positioning enables highly efficient, local mitochondrial Ca^{2+} uptake that overcomes the low affinity Ca^{2+} uptake mechanism known as the mitochondrial Ca^{2+} uniporter (MCU) [10, 11].

In skeletal muscle fibers, mitochondria can be located below the surface membrane (subsarcolemmal), longitudinally between myofibrils (intermyofibrillar), or transversally oriented at the I-band, between triads and Z-lines [12, 13]. The relative abundance of subsarcolemmal, intermyofibrillar or triadic mitochondria depends on fiber type: in glycolytic fast twitch fibers most mitochondria are triadic, whereas subsarcolemmal and inter-myofibrillar mitochondria are more abundant in slower, more oxidative fibers. Similar to that observed in non-excitable cells, electron microscopy (EM) analyses revealed that mitochondria in muscle are tethered ~10 nm long electron dense linkers to the SR. However, mitochondria adjacent to the triad junction are still at least 130 nm from sites of ryanodine receptor mediated Ca^{2+} release [12, 14]. Mitochondrial Ca^{2+} levels increase both *in vitro* [8, 15, 16] and *in vivo* [17] during muscle stimulation. However, the degree to which mitochondrial Ca^{2+} uptake in skeletal muscle depends on microdomain Ca^{2+} signaling has been questioned [14, 16, 18, 19]. As the molecular identity and functional role of the "tether" between the SR and mitochondria in skeletal muscle remains unclear, we evaluated the contribution of Mfn2 to maintaining proper mitochondria Iband localization, association to the SR, as well as mitochondrial morphology, membrane potential, and activity-dependent Ca^{2+} uptake.

Global Mfn2 knockout results in inadequate placental development, delayed maturation, and embryonic lethality [15, 20]. Muscle-specific Mfn1/2 double knockout also results in severe developmental problems and premature death [21]. We circumvented developmental problems and potential compensatory mechanisms to counteract Mfn2 deficiency by using an acute Mfn2 knockdown (KD) approach [22] in FDB muscles of adult (4–5 month old) wild type (WT) mice. High resolution electron and confocal microscopy approaches were used to quantify effects of transient Mfn2 KD on mitochondrial structure and function.

2. Methods

2.1. Animals

Adult (4–5 month old) C57BL/6 WT mice were used in this study. All animals were housed in a pathogen-free area at the University of Rochester School of Medicine and Dentistry. Animals were anesthetized and sacrificed by procedures that were reviewed and approved by the University Committee on Animal Resources at the University of Rochester.

2.2. Chemicals

Mfn2 and non-targeting control (CTRL) siRNAs (siGENOME SMARTpool) were obtained from Dharmacon RNAi Technologies, Thermo Fisher Scientific (Waltham, MA). Cell-permeable, fluorescent Ca^{2+} dyes (rhod-2-AM and mag-fluo-4-AM), membrane permeant Ca^{2+} buffers (EGTA-AM and BAPTA-AM), and tetramethylrhodamine, ethyl ester (TMRE) were obtained from Molecular Probes (Eugene, OR). Collagenase A was obtained from

Roche, USA (Nutley, NJ). Except where indicated otherwise, all other reagents and chemicals were purchased from Sigma-Aldrich (St. Louis, MO).

2.3. Muscle fiber preparation

For experiments involving single muscle fibers, *flexor digitorum brevis* (FDB) muscles were removed from the mouse footpad and acutely dissociated by enzymatic digestion as described previously [23, 24]. Briefly, excised FDB muscles were digested with gentle agitation for 1 hr at 37°C in a rodent Ringer's solution (146mM NaCl, 5mM KCl, 2mM $CaCl_2$, 1mM MgCl, 10mM HEPES, pH 7.4) supplemented with 1 mg/ml collagenase A. Muscles were then suspended in Ringer's without collagenase A and triturated repeatedly using Pasteur pipettes whose tips had been fire-polished to produce openings of successively smaller size. Single FDB fibers were then plated on 35mm glass-bottom dishes and allowed to settle for >30 min before experimentation. Fibers were used within 8 hrs of isolation. All experiments were conducted at room temperature (22–25°C).

2.4. Immunoblotting

Whole FDB muscle lysates or fractions of isolated single fibers after each experiment were saved for immunobloting. To prepare whole FDB muscle lysates, FDB muscles were carefully dissected and homogenized using a Potter homogenizer while on ice in Ripa buffer (1% NP-40, 0.25% NaDOc, 50mM Tris, 150mM HCl, pH 7.4) supplemented with complete protease inhibitors cocktail (Roche, Branford, CT). The homogenate was then solubilized for 1 hr at 4°C with gentle agitation and centrifuged at 13,000 × g for 15 min at 4°C. The supernatant was stored at −80°C until later use. As an alternate approach, acutely dissociated single FDB fibers remaining after completion of functional experiments were collected and solubilized in Ripa buffer as described above. Prior to SDS-PAGE, all samples were diluted in 4× sample buffer (4ml 100%glycerol, 4.8ml 0.5 Tris/HCl pH 6.8, 0.8g SDS, 4mg bromophenol blue, 0.5ml β mercaptaethanol, 0.7ml H_2O). Total protein concentration was determined using the RC DC (reducing agent and detergent compatible) protein assay (BioRad, Hercules, CA). Protein samples (5–10μg) were loaded in each lane and separated using either 4%, 10% or 12% polyacrylamide gels in Tris–Glycine running buffer. The proteins were then transferred onto nitrocellulose membranes (BioRad BioRad, Hercules, CA) overnight at room temperature (RT) or for 1 hr at 4°C in a buffer containing 25mM Tris Base, 191mM Glycine and 20% methanol. The membranes were then blocked with TBST (20mM Tris, 137mM NaCl 0.75% Tween20) plus 5% Blotting Grade Blocker for 1 hr at room temperature and immunostained with primary antibodies: α-Mfn2 (1:1000, Sigma, St. Louis, MO), α-Mfn1 (1:500, Abcam, Cambridge, MA), α-MCU (1:400, Sigma, St. Louis, MO), α-glyceraldehyde 3-phosphate dehydrogenase (GAPDH, 1:10000, Ambion, Austin, TX), α-dihydropyridine receptor (1:300, Thermo Fisher Scientific, Waltham, MA), α-SERCA1 (1:5000, Santa Cruz, Santa Cruz, CA), α-calequestrin1 (CSQ1, 1:1000, Thermo Fisher Scientific, Waltham, MA), ryanodine receptor (34C, University of Iowa, Iowa City, IA), and α-parvalbumin (PV, 1:1000, Abcam, Cambridge, MA), followed by incubation with appropriate goat anti-mouse or anti-rabbit IRDye 800CW secondary antibodies (1:10 000, GE Healthcare, Pittsburgh, PA). Blots were visualized using an ODYSSEY Infrared Imaging System (LI-COR Biosciences, Lincoln, NE). Protein band densitometry was performed using NIH ImageJ software.

2.5. Electroporation of siRNAs in FDB muscle

Acute *in vivo* KD of Mfn2 in skeletal muscle was achieved through electroporation *of* Mfn2-specific siRNAs into footpads of adult mice as described previously [22]. A non-targeting control (CTRL) siRNA was electroporated as control. Briefly, mice were first anesthetized by intramuscular injection of 100 mg/kg ketamine, 10 mg/kg xylazine, and 3 mg/kg acepromazine. Bovine hyaluronidase (2 μg/μl, 8 μl/foot) was then injected subcutaneously into both hind limb footpads. After 1 hr, 400 nmol of siRNA (10 μl total volume suspended in 71 mM NaCl) was similarly injected and the FDB muscle was electroporated (20 ms, 100 V/cm pulses at 1 Hz for 20 s) using gold-plated electrodes placed close to the proximal and distal tendons. Individual FDB fibers were isolated 7 days after electroporation.

2.6. Preparation of samples for Electron microscopy (EM)

For EM experiments, mice were sacrificed by CO_2 inhalation followed by cervical dislocation. Footpad skin was quickly removed and FDB muscles isolated from mice electroporated with CTRL or Mfn2 siRNAs were fixed *in situ* at room temperature with fixative solution (3.5% glutaraldehyde in 0.1 M NaCaCo buffer, pH 7.2) at the University of Rochester and then shipped to University G. d'Annunzio for EM analyses. Small bundles of fixed muscle fibers from FDB muscles were then post-fixed in 2% OsO4 in the same buffer for 2 hr and block-stained in aqueous saturated uranyl acetate. Specimens were rapidly dehydrated in graded ethanol and acetone, infiltrated with Epon 812-acetone (1:1) mixture for 2 hr, and then embedded in Epon. Ultrathin sections (~50 nm) were cut with a Leica Ultracut R (Leica Microsystem, Austria) using a Diatome diamond knife (DiatomeLtd. CH-2501 Biel, Switzerland) and stained in 4% uranyl acetate and lead citrate. Sections were examined with a FP 505 Morgagni Series 268D electron microscope (FEI Company, Brno, Czech Republic) at 60kV equipped with a Megaview III digital camera and AnalySIS software (Olympus Soft Imaging Solutions GmbH, Munster, Germany).

2.7. Quantitative analysis of EM images

Estimates of relative fiber volume occupied by mitochondria and mitochondrial surface area/fiber volume ratio were measured in transversal sections by using the stereology point and intersections counting method as described elsewhere [25]. Briefly, 1–2 micrographs from each fiber were taken at a magnification of 8,900× from cross sections, excluding nuclei and subsarcolemmal regions. Two different types of grids were superimposed to each image: 1) an orthogonal array of dots at a spacing of 0.35 μm and 2) a grid of lines arranged in two orthogonal arrays, separated by a distance of 0.61 μm. The ratio of the numbers of dots falling over a mitochondrion to the total number of dots covering the image was used to approximate relative volume occupied by mitochondria [25, 26]. To estimate mitochondrial surface area, the frequency of intersections between the external profile of the sectioned mitochondria and the grid lines was counted. The ratio of mitochondrial surface area to total fiber volume ($\mu m^2/\mu m^3$) was obtained from the formula $C/2d*Ptest$, where C is the number of intersections between the grid lines and the mitochondria, d is the spacing between the grid lines, and Ptest is the number of grid line intersections in the test area. The denominator, $2d*Ptest$, equals the total length of grid lines in the test grid [27] (Knollman et al., 2006). The extent of mitochondrial network was estimated by measuring the length

(along the long axis) of each individual mitochondrion using the Megaview III digital camera and AnalySIS software (Olympus Soft Imaging Solutions GmbH, Munster, Germany).

2.8. Fiber type analyses

FDB muscle fiber type assessment was performed by silver stain analysis of myosin heavy chain isotypes using a procedure modified from [28]. Briefly, FDB muscles isolated from mice electroporated with CTRL or Mfn2 siRNAs were isolated and homogenized using a Potter homogenizer while in ice-cold homogenization buffer (20mM Imidazole, 150mM KCl, 0.2mM EDTA, pH 7.2 with protease inhibitors). The homogenates were then centrifuged at 13,000 × g for 15 min at 4°C and the pellet resuspended in homogenization buffer (50mM Tris-HCl, 150mM NaCl, pH 7.4 with protease inhibitors). Total protein concentration was determined by RC DC protein assay and 0.2 μg of total protein sample was loaded per lane. Stacking gels were composed of 30% glycerol, 4% acrylamide/bis (49:1), 70 mM Tris (pH 6.7), 4mM EDTA, 0.4% SDS, 0.1% APS and 0.05% TEMED. Separating gels were composed of 35% glycerol, 8% acrylamide/bis (99:1), 0.2 M Tris-HCl (pH 8.8), 0.1 M glycine, and 0.4% SDS, 0.1% APS and 0.05% TEMED. Two separate running buffers were used for the inner and outer chambers. The outer chamber running buffer consisted of 0.05M Tris, 0.075M glycine and 0.05% SDS. The inner chamber running buffer was an 8× concentration of the outer running buffer supplemented with 0.12% β-mercaptoethanol. Inner and outer chamber buffers were cooled to 4°C before use. The running conditions were 140 V for 20 hr. The gels were visualized by silver staining (Biorad, Hercules, CA silver stain plus kit, according to the kit manuals) and were photographed using a BioRad imaging scanner. Densitometry analysis of the protein bands was carried out using Image Lab 4.0.1 software (BioRad, Hercules, CA).

2.9. Mitochondrial membrane potential measurements

Single FDB fibers isolated from mice electroporated with CTRL or Mfn2 siRNAs were loaded with 20nM tetramethylrhodamine methyl ester (TMRE), a fluorescent indicator of the mitochondrial membrane potential ($\Delta\Psi$), for 20 min at room temperature. The TMRE concentration was then diluted 1:2 and maintained throughout the experiment. TMRE was excited using a 543nm laser and fluorescence images were acquired using a confocal microscope (Nikon Eclipse C1 Plus, Melville, NY) equipped with a 40× 1.3 numerical aperture (NA) oil objective. Sequential images were taken at 15 sec intervals. 1 μM FCCP perfusion was started 45 seconds after the start of the time series and TMRE fluorescence decay was monitored as an indicator of dissipation of the mitochondrial membrane potential.

A titration of FCCP concentration was performed to determine the FCCP concentration needed to reduce TRME fluorescence of fibers from WT mice to ~50% of control [29, 30]. Time-lapsed images (15 frames for total 8 min at 15 sec intervals) were acquired before and after 5 min incubation with 20nM, 50nM, and 100nM FCCP. Frames 1–3 were taken at rest, followed by 5 minutes in the presence of 0, 20nM, 50nM, or 100nM FCCP with no images taken, then 12 successive images were taken to follow the decay of TMRE fluorescence while perfusing 1μM FCCP to completely dissipate $\Delta\Psi$.

2.10. Confocal imaging/analysis of mitochondrial Ca^{2+} uptake during tetanic stimulation

Activity-dependent changes in myoplasmic and mitochondrial Ca^{2+} levels in single FDB fibers were monitored with mag-fluo-4 and rhod-2, respectively [16]. Briefly, FDB fibers isolated from mice electroporated with CTRL or Mfn2 siRNAs were loaded with 5 μM rhod 2-AM for 30 min at room temperature, followed by 4 μM mag-fluo-4-AM for 20 min at room temperature. Fibers were then washed in dye-free solution supplemented with 25 μM N-benzylp-toluene sulfonamide (BTS) for 20 min to block contractions (8, 28). Fibers were electrically stimulated with a series of 5 consecutive tetani (500 ms duration, 100 Hz, 0.2 duty cycle) using an extracellular stimulation electrode filled with 200 mM NaCl placed adjacent to the cell of interest. Mag-fluo-4 (myoplasmic Ca^{2+}) and rhod-2 (mitochondrial Ca^{2+}) were sequentially excited using 488nm and 543nm lasers and fluorescence emission was detected at 515/30nm and 610/75 nm, respectively. Time series *x-y* images (256 × 256 pixels/frame, 0.2 μm/pixel, 690-ms scan duration, with variable delays) were acquired using a confocal microscope (Nikon Instruments, Melville, NY). Mag-fluo-4 fluorescence was monitored during electrical stimulation, immediately followed by measurements of rhod-2 fluorescence (690 ms after initiation of electrical stimulation). Images were taken at rest, during the 1^{st} and 5^{th} tetanus, every 5 sec for 2 min, and then finally every 30 sec for the next 8 minutes. The effects of slow (EGTA) and fast (BAPTA) Ca^{2+} chelators on mitochondrial Ca^{2+} uptake were performed as described above, except that following dye loading, FDB fibers were incubated for an additional 30 minutes in solution supplemented with either 25μM EGTA-AM or 25μM BAPTA-AM.

Imaging data were analyzed offline using NIH ImageJ and Igor Pro software (WaveMetrics Inc., Lake Oswego, OR). Calculation of mean rhod-2 fluorescence values representing mitochondria localized to the triad was performed as described previously [16]. Briefly, a 2 μm line was drawn along the longitudinal axis of the fiber (x values corresponded to fiber length and y values corresponded to averaged fluorescence levels). Triadic mitochondrial rhod-2 fluorescence was calculated as the differences between the peaks (I band fluorescence, representing mitochondria) and troughs (A band, non-mitochondrial fluorescence, baseline). Relative mitochondrial Ca^{2+} uptake was expressed as F/F_0, where F_0 is the peak (I-band) minus trough (A-band) fluorescence before stimulation.

2.11. Mag-fluo4 photometry measurements of myoplasmic Ca^{2+}

A low affinity Ca^{2+} dye and a rapid photon counting system were used to optimally resolve the magnitude and kinetics of electrically-evoked Ca^{2+} release in single FDB fibers [31]. Briefly, FDB fibers were loaded with 4 μM mag-fluo-4-AM for 20 min at room temperature followed by washout in dye-free solution supplemented with 25 μM N-benzylp-toluene sulfonamide for 20 min. Fibers were electrically stimulated with a series of either twitch stimulations (1 ms pulse at 2 Hz) or 5 consecutive tetani (500 ms at 100 Hz, 0.2 duty cycle) using an extracellular electrode placed adjacent to the cell of interest. Mag-fluo-4 was excited at 480±15nm using an Excite epifluorescence illumination system (Nikon Instruments, Melville, NY) and fluorescence emission at 535±30nm was monitored with a 40× oil objective and a photomultiplier detection system (Photon Techniologies Incorporated, Birmingham, NJ). Relative changes in mag-fluo-4 fluorescence from baseline (F/F_0) were recorded at 10kHz using Clampex 9.0 (Molecular Devices, Burlingame, CA).

2.12. Confocal line-scan imaging and analysis of mitochondrial-targeted ratiometric pericam fluorescence during twitch stimulation

Mitochondrial-targeted ratiometric pericam (mt-pericam) fluorescence was monitored in FDB fibers from mice electroporated with either CTRL or Mfn2 siRNAs as described previously [16]. A series of electrically-evoked twitches (1 ms pulse at 0.5Hz) were elicited using an extracellular electrode. Real-time changes in relative mt-pericam fluorescence during individual twitches were monitored by confocal line scan (2 ms/line, 1,024 lines) across a 50-μm line drawn along the longitudinal axis of the fiber. Mt-pericam was excited using a 402 nm laser and emission collected at 515±30 nm. Images were analyzed offline using NIH ImageJ software. Relative changes in mt-pericam fluorescence (ΔF/F) during twitch stimulation were assessed within a 1 μm thick line corresponding to the mt-pericam fluorescence within the I band [16].

2.13. Measurements of total Ca^{2+} store content

FDB fibres were loaded with 4 μM fura-2FF-AM at room temperature for 30 min followed by a 30 min washout in dye free Ringer's solution. Total Ca^{2+} store content was determined by the change in fura2-FF fluorescence during local application of a Ca^{2+} release cocktail consisting of 10 μM ionomycin, 30 μM cyclopiazonic acid (CPA), and 100 μM EGTA/0 Ca^{2+}) [31].

2.14. Statistics

To enable comparison between different fibers within each experiment, confocal images were recorded using identical laser power, photomultiplier sensitivity, and were processed using identical values for contrast and brightness. Statistical significance between relative changes in myoplasmic mag-fluo-4 fluorescence and mitochondrial rhod-2 and mt-pericam fluorescence were determined using one-way ANOVA with Dunn's post-hoc tests. For the comparison between only two groups of data Student's t-test was used. Throughout this study, statistical significance was taken as $p < 0.05$.

3. Results

3.1. Mitofusin2 knockdown (KD)

Mfn2 specific siRNAs or non-targeting CTRL siRNAs were electroporated into anesthetized 4–5 month old wild type C57Bl6 mice (see Methods). A 67±3% (n=10) reduction in Mfn2 protein expression was achieved 7 days after electroporation (Fig.1A and 1B). Short-term Mfn2 KD did not alter expression of mitofusin1 (Mfn1) or several critical proteins involved in Ca^{2+} regulation in skeletal muscle including the mitochondrial Ca^{2+} uniporter (MCU), the dihydropyridine receptor (DHPR), the sarco/endoplasmic reticulum Ca^{2+} ATPase (SERCA1), the type 1 SR Ca^{2+} binding protein calsequestrin (CASQ1), the type I ryanodine receptor (RyR1), or the myoplasmic Ca^{2+} binding protein parvalbumin (PV) (Fig. 1A and B). Myosin heavy chain analysis showed no change in fiber type composition in FDB muscles following Mfn2 KD (Fig. 1C and D, 80% type IIa/x and 20% type I [32, 33]).

3.2. Mitochondrial morphology and localization is altered in Mfn2 KD FDB fibers

No significant difference in total mitochondrial volume was found between CTRL and Mfn2 KD fibers (Table 1, column A). However, qualitative analyses revealed several significant changes in mitochondrial morphology (Fig. 2). In CTRL FDB muscle fibers, mitochondria in proximity to Z lines (in cross sections) appeared elongated and primarily located at the "I band" (Fig. 2 A), with only rare instances of mitochondria being located within the A band region of the sarcomere (Fig. 2B). Following Mfn2 KD, mitochondrial surface/volume ratio was significantly reduced (Table 1, column B) and the percentage of mitochondria located within the A-band region increased significantly (Fig. 2C and Table 1, column C). In addition, these mitochondria appeared more rounded and mis-oriented (Fig. 2D). Qualitative EM analyses of FDB muscle cross sections revealed that average mitochondrial aspect ratio and form factor were significantly reduced following Mfn2 KD (Fig. 2E and F). Thus, Mfn2 KD reduced mitochondrial length and branching, consistent with increased mitochondrial fragmentation..

3.3. Mfn2 KD reduces SR-mitochondrial tethering

In adult fast twitch skeletal muscle fibers, mitochondria are primarily located in close proximity to Ca^{2+} release units (CRUs) [12]. Following Mfn2 KD, the number of mitochondria localized close to CRUs was significantly reduced compared to that observed in CRTL (Table 2, column A). This finding, combined with the increased frequency of mitochondria located in the A band region of the sarcomere (Table 1, column C), suggests that Mfn2 KD promotes detachment of some mitochondria from the CRU. While the number of tethers in the remaining mitochondrial-CRU pairs was not altered (Table 2, column B and Supplemental Fig. 1), overall tether density per fiber area was also significantly reduced with Mfn2 KD (Table 2, column C).

3.4. Mfn2 KD reduces activity-dependent mitochondrial Ca^{2+} uptake and increases the global myoplasmic Ca^{2+} transient

Since mitochondrial morphology and tethering to the SR were altered in Mfn2 KD muscles, we measured mitochondrial Ca^{2+} uptake elicited by a train of five consecutive high frequency tetanic stimulations (500 ms, 100 Hz, 0.2 duty cycle) [16]. Mitochondrial Ca^{2+} uptake following the fifth tetanus was reduced by ~40% in Mfn2 KD fibers compared to that of CTRL fibers (Fig. 3A and B). This reduction in mitochondrial Ca^{2+} uptake in Mfn2 KD fibers occurred in parallel with a significant increase in the magnitude of the global myoplasmic Ca^{2+} transient (Fig. 3C and D). Similarly, mitochondrial Ca^{2+} uptake was also significantly reduced (Fig. 4A and B) and the myoplasmic Ca^{2+} transient increased (Fig. 4C and D) in Mfn2 KD fibers during single twitch stimulation. Mfn2 KD did not alter total Ca^{2+} store content assessed using a Ca^{2+} release cocktail consisting of 10 μM ionomycin, 30 μM CPA, and 100 μM EGTA/0 Ca^{2+} (Fig. 3E).

3.5 Mfn2 KD results in depolarization of the mitochondrial membrane potential

The mitochondrial membrane potential ($\Delta\Psi_m$) is a critical determinant of the driving force for mitochondrial Ca^{2+} uptake. To determine if depolarization in $\Delta\Psi_m$ underlies the reduction in mitochondrial Ca^{2+} uptake observed in Mfn2 KD fibers, we measured the

FCCP-sensitive mitochondrial membrane potential in FDB fibers loaded with 20nM TMRE. FDB fibers loaded with TMRE exhibited clear double rows of transverse TMRE fluorescence, consistent with efficient loading of the dye into I-band delimited mitochondria. Addition of 1 μM FCCP resulted in a time-dependent and complete dissipation of TMRE fluorescence (Fig. 5A and B). Both the basal (Fig. 5C) and FCCP-sensitive TMRE responses (Fig. 5D) were significantly reduced in Mfn2 KD fibers compared to that observed for CTRL FDB fibers, consistent with a significant depolarization of the $\Delta\Psi_m$ with Mfn2 KD.

3.6 $\Delta\Psi_m$ depolarization is sufficient to reduce activity-dependent mitochondrial Ca^{2+} uptake

To more rigorously determine the relative contribution of the $\Delta\Psi_m$ to activity-dependent mitochondrial Ca^{2+} uptake in FDB fibers, we induced graded $\Delta\Psi_m$ depolarization in wild-type FDB fibers by pre-incubating fibers for 5 min in different concentrations (20 nM, 50 nM, and 100 nM) of FCCP (Supplemental Figure 1). While no significant effect on TMRE fluorescence was observed with 20 nM FCCP, a significant concentration-dependent effect on both basal TMRE fluorescence and maximal FCCP-induced change in TMRE fluorescence was observed for 50 nM and 100 nM FCCP. In fact, pretreatment of FDB fibers with 50 nM FCCP produced a comparable reduction in TMRE fluorescence as that observed following Mfn2 KD (compare Figs. 5D and Supplemental Figure 1C). Importantly, activity-dependent mitochondrial Ca^{2+} uptake was reduced to similar levels in both Mfn2 KD fibers and CRTL fibers pretreated for 5 minutes with 50 nM FCCP (Fig. 6B). Moreover, preincubation of Mfn2 KD fibers with 50 nM FCCP resulted in a further reduction in activity-dependent mitochondrial Ca^{2+} uptake (Fig. 6A and B) and a parallel increase in the magnitude of the global myoplasmic Ca^{2+} transient (Fig. 6C and D).

3.7 Buffering of global myoplasmic Ca^{2+} reduces activity-dependent mitochondrial Ca^{2+} uptake

To better evaluate the validity of the “microdomain” theory for mitochondrial Ca^{2+} uptake in adult skeletal muscle, we performed a series of mitochondrial Ca^{2+} uptake measurements in the presence of either intracellular EGTA (a slow Ca^{2+} chelator) or BAPTA (a fast Ca^{2+} chelator). Due to its faster kinetics and ability to interact with membrane phospholipids, BAPTA chelates Ca^{2+} ions within a much shorter length constant (~30nm) compared to that for EGTA (~100nm) [34–36]. Following 30 minute incubation in either 25μM EGTA-AM or 25μM BAPTA-AM, myoplasmic Ca^{2+} transients and mitochondrial Ca^{2+} uptake were monitored during 5 successive tetanic stimulations (Fig. 7). EGTA-AM pretreatment reduced peak electrically-evoked myoplasmic Ca^{2+} transients by ~20% and maximal mitochondrial Ca^{2+} uptake by ~65%. On the other hand, incubation with BAPTA-AM resulted in a significantly larger reduction in both the peak electrically-evoked myoplasmic Ca^{2+} transient (~40%) and maximal mitochondrial Ca^{2+} uptake (>90%). Similar results were observed for both chelators in Mfn2 KD fibers (Fig. 7). The parallel inhibition of both the global myoplasmic Ca^{2+} transient and mitochondrial Ca^{2+} uptake by EGTA and BAPTA indicate that the mitochondrial Ca^{2+} uptake mechanisms in FDB fibers respond primarily to changes in the global, rather than microdomain, Ca^{2+} as suggested previously [16].

4. Discussion

This study provides a comprehensive analysis of the role of Mfn2 in mitochondrial morphology, subcellular location, and function in adult skeletal muscle. Our results demonstrate that transient knockdown of Mfn2 in skeletal muscle leads to mitochondrial fragmentation, mis-localization from the triad and a reduction in both mitochondrial membrane potential and activity-dependent mitochondrial Ca^{2+} uptake. In addition, results using intracellular Ca^{2+} buffers indicate that the mitochondrial Ca^{2+} uptake mechanisms in skeletal muscle respond primarily to changes in the bulk myoplasmic Ca^{2+} pool. These findings provide new insight into the role of Mfn2 in the mechanisms that control activity-dependent mitochondrial Ca^{2+} uptake in skeletal muscle.

In non-excitable cells, mitochondrial juxtaposition to the ER is believed to be essential for proper mitochondrial Ca^{2+} uptake from a microdomain Ca^{2+} pool that builds up in close proximity (~ 10 nm) to sites of Ca^{2+} release [8]. This intimate contact between the two organelles in HeLa and mouse liver cells is maintained through formation of electron dense tethers that intimately connect mitochondria to the ER [6]. Tethers were found to be formed by association of Mfn1 and/or Mfn2 monomers in mitochondria forming homo/hetero-dimers with Mfn2 in the ER through interactions between mitofusin C terminal heptad repeats. Similar tethers were identified in cardiac [37] and skeletal muscle fibers [12]. However, the obligate role of microdomain Ca^{2+} signaling in mitochondrial Ca^{2+} uptake in muscle is unclear since mitochondria are located >130 nm away from sites of RyR1-mediated Ca^{2+} release, a distance that lies further away from the conceptually accepted 10 nm domain of highly elevated Ca^{2+} close to the Ca^{2+} release channel. This distance, however, still places mitochondria within the region where Ca^{2+} is elevated approximately 3 times above the global myoplasmic level during myoplasmic Ca^{2+} transient in skeletal muscle, outside that required for privileged microdomain signaling [14, 38]. Here, we provide evidence from acute KD experiments that Mfn2 comprises an important component of the tethering element linking mitochondria to the CRU in skeletal muscle. In addition to this structural role, Mfn2 also influences mitochondrial morphology and the ability of mitochondria to maintain a $\Delta\Psi_m$ required for maximal activity-dependent mitochondrial Ca^{2+} uptake. Moreover, results from EGTA/BATPA experiments indicate that the mitochondrial Ca^{2+} uptake mechanisms respond to the global myoplasmic Ca^{2+} transient rather than a privileged SR-mitochondrial Ca^{2+} microdomain.

A major population of the mitochondria in adult, fast twitch skeletal muscle fibers are positioned within the “I band”, adjacent to the junctional SR or triad, where the CRUs are located (“triadic mitochondria”). These mitochondria appear as transversally elongated organelles that can span a few sarcomeres and engulf myofibrils [12, 13]. Our results confirmed fragmented, more circular mitochondria (Fig. 2, Table 1) and reduced tether density (Table 2) following acute *in vivo* Mfn2 KD, consistent with previous studies in non-excitable cells [6]. Thus, mitochondrial morphology, triad localization, and SR tethering in muscle are also dependent on Mfn2. Previous studies in muscle from Mfn2 knockout mice found constitutive Mfn2 deficiency resulted in mitochondrial aggregation, fragmentation, enlargement, and clustering [21]. Importantly, we did not observe marked mitochondrial aggregation following acute Mfn2 KD in adult muscle like that observed in Mfn2 knockout

mice, suggesting that aggregation either requires more prolonged Mfn2 deficiency or that sufficient Mfn2-Mfn1 mediated fusion persisted following Mfn2 KD in our experiments.

The significant reduction in tether frequency (Table 2) and increase in non-tethered mitochondrial in the A-band region of the sarcomere (Table 1) is consistent with Mfn2 playing a role in tethering mitochondria to the CRU in muscle. However, since our acute Mfn2 KD approach did not completely abolish Mfn2 protein expression (~70% reduction), it is likely that the tethers remaining following KD reflect hetero-oligomers of low levels of Mfn2 with normal levels of Mfn1. There is also a possibility that other proteins contribute to tether formation in skeletal muscle, such as endoplasmic reticulum - mitochondria encounter structures (or “ERMES”) that are observed in yeast. However, it is currently unclear if such structures are present in mammalian cells [39]. The significant increase in the percentage of mitochondria mis-localized to the “A band” region and decrease in the frequency of mitochondria-CRU pairs is consistent with disruption of tethering to CRUs. Alternatively, it is possible that detachment of mitochondria from the SR could result in elongated mitochondria becoming shorter, retracted, and more rounded such that they are capable of migrating and occupying the limited intermyofibrillar space available within the A band region of the sarcomere.

Our functional studies revealed that mitochondrial Ca^{2+} uptake during repetitive tetanic stimulation is significantly reduced and myoplasmic Ca^{2+} levels are elevated in Mfn2 KD fibers (Fig. 3). These results are consistent with the myoplasmic Ca^{2+} transient during strenuous activity being modestly buffered by mitochondrial Ca^{2+} uptake. The sustained increase in mitochondrial Ca^{2+} following repetitive tetanic stimulation (taking >10 minutes to fully decline) is ideally suited to promote Ca^{2+} activation of mitochondrial ATP generation as suggested previously [16]. We also found that resting $\Delta\Psi_m$ was more depolarized in Mfn2 KD fibers compared to that observed in fibers from control mice (Fig. 5) and that a similar reduction mitochondrial Ca^{2+} uptake is observed when a comparable degree of $\Delta\Psi_m$ depolarization is induced by acute addition of a low concentration (50 nM) of FCCP (Fig. 6 and Supplemental Fig. 2). These findings indicate that the reduction in activity-dependent Ca^{2+} uptake in triadic mitochondria following Mfn2 KD fibers is largely a result of the depolarization of $\Delta\Psi_m$ reducing the electrical driving force for mitochondrial Ca^{2+} uptake rather than a change in Ca^{2+} transport capacity. Indeed, MCU expression was not altered following short-term Mfn2 KD. The depolarization in $\Delta\Psi_m$ and mitochondrial fragmentation observed here following Mfn2 KD are consistent with the mitochondrial fragmentation and $\Delta\Psi_m$ depolarization reported previously in skeletal muscle from a mouse model of amyotrophic lateral sclerosis [40].

In cardiac myocytes [41, 42] and non-excitable cells [9, 43], mitochondrial Ca^{2+} uptake persists even after buffering the global cytoplasmic Ca^{2+} transient with EGTA or BAPTA, consistent with the mitochondrial Ca^{2+} uptake channels being located within a privileged Ca^{2+} release microdomain. On the other hand, triadic mitochondria in adult skeletal muscle are no closer than 130 nm from sites of RyR1 Ca^{2+} release [12, 13]. Thus, we determined the effect of buffering the myoplasmic Ca^{2+} on activity-dependent mitochondrial Ca^{2+} uptake in FDB fibers. Loading FDB fibers with EGTA or BAPTA resulted in parallel reductions in both the global myoplasmic Ca^{2+} transient and mitochondrial Ca^{2+} uptake

(Fig. 7). The stronger effect of BAPTA in these experiments was not unexpected given its faster kinetics of Ca^{2+} binding. These results, and particularly the significant buffering of mitochondrial Ca^{2+} uptake by EGTA, provide strong evidence that the Ca^{2+} uptake mechanisms in triadic mitochondria respond to the bulk myoplasmic Ca^{2+} pool rather than a privileged local Ca^{2+} release microdomain. This assertion is supported by our previous observation that activity dependent mitochondrial Ca^{2+} uptake is similar in triadic mitochondria and clusters of longitudinal mitochondria in FDB fibers from young mice, in spite of the fact that mitochondria in longitudinal clusters are positioned even further away from sites of RyR1 Ca^{2+} release [16]. While the relatively low affinity of the mitochondrial Ca^{2+} uniporter limits the degree of mitochondrial Ca^{2+} uptake that can be achieved during repetitive tetanic stimulation, this limitation may be mitigated in skeletal muscle due to the high level of functional uniporter channel activity observed in this tissue (e.g. ~30× larger than MCU channel activity in the heart) [44].

In summary, our results indicate that Mfn2 is an important determinant of mitochondrial localization, morphology, and tethering to the CRU in skeletal muscle. In addition, Mfn2 KD results in a marked reduction in Ca^{2+} uptake by mitochondria remaining associated with the triad junction and this reduction is due largely to a depolarization of the mitochondrial membrane potential rather than a decrease in either the myoplasmic global Ca^{2+} transient or expression of the mitochondrial Ca^{2+} uniporter. Finally, consistent with measurements of the distance between triadic mitochondria and sites of RyR1 Ca^{2+} release [12] and modeling of the Ca^{2+} release microdomain in muscle [14], our EGTA/BAPTA results indicate that the mitochondrial Ca^{2+} uptake mechanisms in skeletal muscle respond primarily to changes in global Ca^{2+} and not a privileged Ca^{2+} microdomain.

Supplementary Material

Refer to Web version on PubMed Central for supplementary material.

Acknowledgements

This work also was supported by grants from NIH (AR059646) and MDA (MDA275574) to RTD and the Italian Telethon Foundation to FP. The sponsors played no role in the study design, data collection, analysis, interpretation, or writing of this report.

Abbreviations

WT	Wild Type
FCCP	Carbonylcyanide-p-trifluoromethoxyphenylhydrazone
CRU	Calcium Release Unit
CTRL	Control
ER/SR	Endopla smic/Sarcoplasmic Reticulum
FDB	Flexor Digitorum Brevis
KD	Knockdown

MCU	Mitochondrial Ca^{2+} Uniporter
Mfn1/2	Mitofusin 1/2
TMRE	Tetramethylrhodamine Methyl Ester

References

1. Westerblad H, Bruton JD, Katz A. Skeletal muscle: energy metabolism, fiber types, fatigue and adaptability. Exp Cell Res. 2010; 316(18):3093–3099. [PubMed: 20580710]
2. Zurlo F, et al. Skeletal muscle metabolism is a major determinant of resting energy expenditure. J Clin Invest. 1990; 86(5):1423–1427. [PubMed: 2243122]
3. Heymsfield SB, et al. Body-size dependence of resting energy expenditure can be attributed to nonenergetic homogeneity of fat-free mass. Am J Physiol Endocrinol Metab. 2002; 282(1):E132–E138. [PubMed: 11739093]
4. Hoppins S, Lackner L, Nunnari J. The machines that divide and fuse mitochondria. Annu Rev Biochem. 2007; 76:751–780. [PubMed: 17362197]
5. Santel A, Fuller MT. Control of mitochondrial morphology by a human mitofusin. J Cell Sci. 2001; 114(Pt 5):867–874. [PubMed: 11181170]
6. de Brito OM, Scorrano L. Mitofusin 2 tethers endoplasmic reticulum to mitochondria. Nature. 2008; 456(7222):605–610. [PubMed: 19052620]
7. Merkwirth C, Langer T. Mitofusin 2 builds a bridge between ER and mitochondria. Cell. 2008; 135(7):1165–1167. [PubMed: 19109886]
8. Yi J, et al. Mitochondrial calcium uptake regulates rapid calcium transients in skeletal muscle during excitation-contraction (E-C) coupling. J Biol Chem. 2011; 286(37):32436–32443. [PubMed: 21795684]
9. Rizzuto R, et al. Microdomains with high Ca2+ close to IP3-sensitive channels that are sensed by neighboring mitochondria. Science. 1993; 262(5134):744–747. [PubMed: 8235595]
10. Bragadin M, Pozzan T, Azzone GF. Kinetics of Ca2+ carrier in rat liver mitochondria. Biochemistry. 1979; 18(26):5972–5978. [PubMed: 42437]
11. Patergnani S, et al. Calcium signaling around Mitochondria Associated Membranes (MAMs). Cell Commun Signal. 2011; 9:19. [PubMed: 21939514]
12. Boncompagni S, et al. Mitochondria are linked to calcium stores in striated muscle by developmentally regulated tethering structures. Mol Biol Cell. 2009; 20(3):1058–1067. [PubMed: 19037102]
13. Ogata T, Yamasaki Y. Scanning electron-microscopic studies on the three-dimensional structure of mitochondria in the mammalian red, white and intermediate muscle fibers. Cell Tissue Res. 1985; 241(2):251–256. [PubMed: 4028126]
14. Dirksen RT. Sarcoplasmic reticulum-mitochondrial through-space coupling in skeletal muscle. Appl Physiol Nutr Metab. 2009; 34(3):389–395. [PubMed: 19448704]
15. Bruton J, et al. Mitochondrial and myoplasmic [Ca2+] in single fibres from mouse limb muscles during repeated tetanic contractions. J Physiol. 2003; 551(Pt 1):179–190. [PubMed: 12815178]
16. Rossi AE, et al. Differential impact of mitochondrial positioning on mitochondrial Ca(2+) uptake and Ca(2+) spark suppression in skeletal muscle. Am J Physiol Cell Physiol. 2011; 301(5):C1128–C1139. [PubMed: 21849670]
17. Rudolf R, et al. In vivo monitoring of Ca(2+) uptake into mitochondria of mouse skeletal muscle during contraction. J Cell Biol. 2004; 166(4):527–536. [PubMed: 15314066]
18. Shkryl VM, Shirokova N. Transfer and tunneling of Ca2+ from sarcoplasmic reticulum to mitochondria in skeletal muscle. J Biol Chem. 2006; 281(3):1547–1554. [PubMed: 16216882]
19. Franzini-Armstrong C. ER-mitochondria communication. How privileged? Physiology (Bethesda). 2007; 22:261–268. [PubMed: 17699879]

20. Chen H, et al. Mitofusins Mfn1 and Mfn2 coordinately regulate mitochondrial fusion and are essential for embryonic development. J Cell Biol. 2003; 160(2):189–200. [PubMed: 12527753]
21. Chen H, et al. Mitochondrial fusion is required for mtDNA stability in skeletal muscle and tolerance of mtDNA mutations. Cell. 2010; 141(2):280–289. [PubMed: 20403324]
22. DiFranco M, et al. DNA transfection of mammalian skeletal muscles using in vivo electroporation. J Vis Exp. 2009; (32)
23. Beam KG, Knudson CM. Calcium currents in embryonic and neonatal mammalian skeletal muscle. J Gen Physiol. 1988; 91(6):781–798. [PubMed: 2458429]
24. Lueck JD, et al. Muscle chloride channel dysfunction in two mouse models of myotonic dystrophy. J Gen Physiol. 2007; 129(1):79–94. [PubMed: 17158949]
25. Mobley BA, Eisenberg BR. Sizes of components in frog skeletal muscle measured by methods of stereology. J Gen Physiol. 1975; 66(1):31–45. [PubMed: 1159401]
26. Loud AV, Barany WC, Pack BA. Quantitative Evaluation of Cytoplasmic Structures in Electron Micrographs. Lab Invest. 1965; 14:996–1008. [PubMed: 14317063]
27. Knollmann BC, et al. Casq2 deletion causes sarcoplasmic reticulum volume increase, premature Ca2+ release, and catecholaminergic polymorphic ventricular tachycardia. J Clin Invest. 2006; 116(9):2510–2520. [PubMed: 16932808]
28. Talmadge RJ, Roy RR. Electrophoretic separation of rat skeletal muscle myosin heavy-chain isoforms. J Appl Physiol. 1993; 75(5):2337–2340. [PubMed: 8307894]
29. Brennan JP, et al. Mitochondrial uncoupling, with low concentration FCCP, induces ROS-dependent cardioprotection independent of KATP channel activation. Cardiovasc Res. 2006; 72(2):313–321. [PubMed: 16950237]
30. Brennan JP, et al. FCCP is cardioprotective at concentrations that cause mitochondrial oxidation without detectable depolarisation. Cardiovasc Res. 2006; 72(2):322–330. [PubMed: 16979603]
31. Loy RE, et al. Muscle weakness in Ryr1I4895T/WT knock-in mice as a result of reduced ryanodine receptor Ca2+ ion permeation and release from the sarcoplasmic reticulum. J Gen Physiol. 2011; 137(1):43–57. [PubMed: 21149547]
32. Calderón J, et al. Different fibre populations distinguished by their calcium transient characteristics in enzymatically dissociated murine <i>flexor digitorum brevis</i> and <i>soleus</i> muscles. Journal of Muscle Research and Cell Motility. 2009; 30(3): 125–137. [PubMed: 19543797]
33. González E, et al. Insulin-like growth factor-1 prevents age-related decrease in specific force and intracellular Ca2+ in single intact muscle fibres from transgenic mice. The Journal of Physiology. 2003; 552(3):833–844. [PubMed: 12937290]
34. Rousset M, et al. Ca2+-dependent interaction of BAPTA with phospholipids. FEBS Lett. 2004; 576(1–2):41–5. [PubMed: 15474007]
35. Putney, JW. Methods in signal transduction. 2nd ed.. Boca Raton: CRC/Taylor & Francis; 2006. Calcium signaling; p. 509
36. Naraghi M, Neher E. Linearized buffered Ca2+ diffusion in microdomains and its implications for calculation of [Ca2+] at the month of a calcium channel. Journal of Neuroscience. 1997; 17(18): 6961–6973. [PubMed: 9278532]
37. Garcia-Perez C, et al. Alignment of sarcoplasmic reticulum-mitochondrial junctions with mitochondrial contact points. Am J Physiol Heart Circ Physiol. 2011; 301(5):H1907–H1915. [PubMed: 21856920]
38. Baylor SM, Hollingworth S. Simulation of Ca2+ movements within the sarcomere of fast-twitch mouse fibers stimulated by action potentials. J Gen Physiol. 2007; 130(3):283–302. [PubMed: 17724162]
39. Kornmann B, et al. An ER-mitochondria tethering complex revealed by a synthetic biology screen. Science. 2009; 325(5939):477–481. [PubMed: 19556461]
40. Luo G, et al. Defective mitochondrial dynamics is an early event in skeletal muscle of an amyotrophic lateral sclerosis mouse model. PLoS One. 2013; 8(12):e82112. [PubMed: 24324755]
41. Sharma VK, et al. Transport of Ca2+ from sarcoplasmic reticulum to mitochondria in rat ventricular myocytes. J Bioenerg Biomembr. 2000; 32(1):97–104. [PubMed: 11768767]

42. Szalai G, et al. Calcium signal transmission between ryanodine receptors and mitochondria. J Biol Chem. 2000; 275(20):15305–15313. [PubMed: 10809765]

43. Csordas G, et al. Imaging interorganelle contacts and local calcium dynamics at the ER-mitochondrial interface. Mol Cell. 2010; 39(1):121–132. [PubMed: 20603080]

44. Fieni F, et al. Activity of the mitochondrial calcium uniporter varies greatly between tissues. Nat Commun. 2012; 3:1317. [PubMed: 23271651]

Highlights

- Mfn2 knockdown in muscle causes mitochondrial fragmentation and mis-localization.
- Mfn2 knockdown in muscle reduces mitochondrial Ca^{2+} uptake.
- Mfn2 knockdown in muscle depolarizes the mitochondrial membrane potential.
- Mitochondria in muscle respond to changes in the bulk myoplasmic Ca^{2+} pool.
- Mfn2 is required for optimal mitochondrial Ca^{2+} uptake in skeletal muscle.

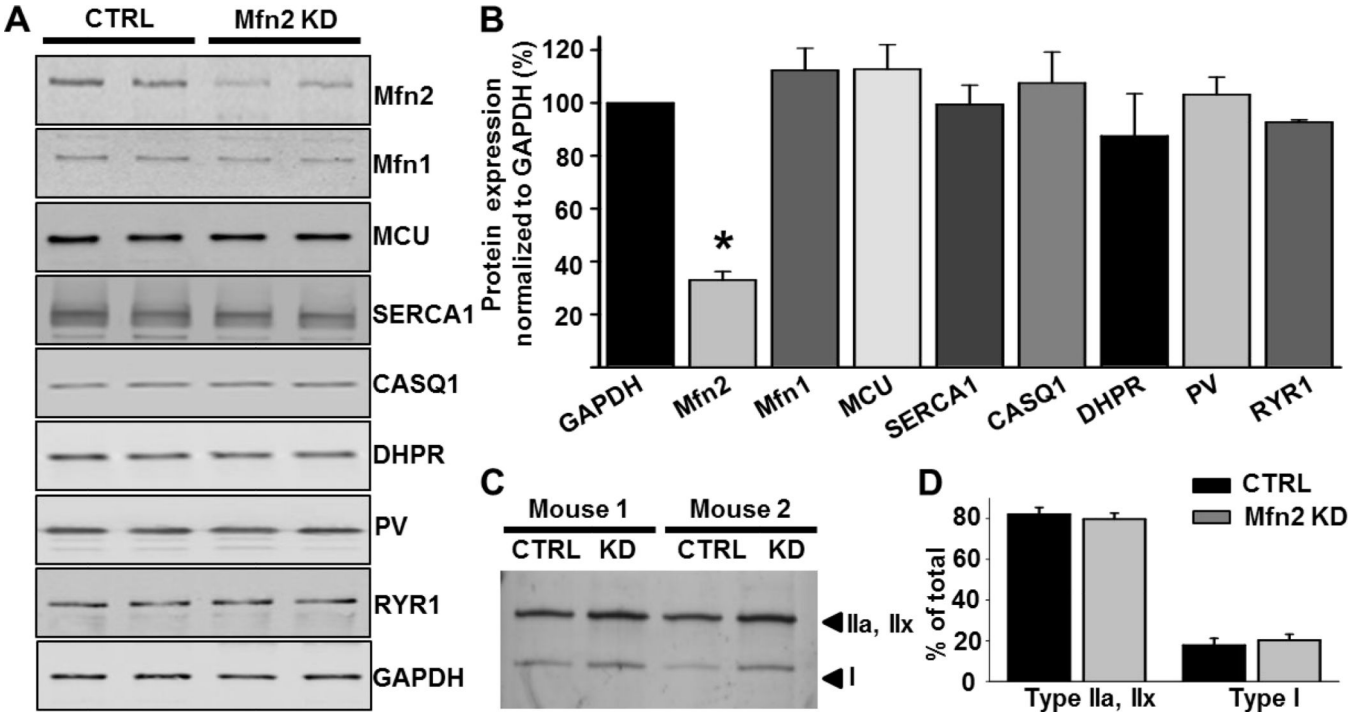

Figure 1.

Quantification of expression levels of proteins involved in Ca^{2+} regulation in skeletal muscle following short-term Mfn2 knockdown. A. Representative western blots against Mfn1, Mfn2 and proteins involved in Ca^{2+} regulationin FDB muscles electroporated with CTRL or Mfn2 siRNAs. Mfn2 KD did not significantly alter expression levels of the DHPR, SERCA1, Mfn1, CASQ1, MCU or PV. B. Average (±SE) protein expression levels in CTRL and Mfn2 KD muscles. Mfn2 expression was reduced 67±3% in FDB muscles electroporated with Mfn2 siRNAs (N=10, $P<0.05$) compared to CTRL. DHPR, SERCA1, Mfn1, CASQ1, RyR1, MCU and PV levels were unaltered. C. Silver stain blot of the distribution of myosin heavy chain isotypes in CTRL and Mfn2 KD FDB muscles. D. Average (±SE) percent distribution of myosin heavy chain isotypes in CTRL and Mfn2 KD FDB muscles. No significant difference in fiber typing was observed between CTRL and Mfn2 KD muscles.

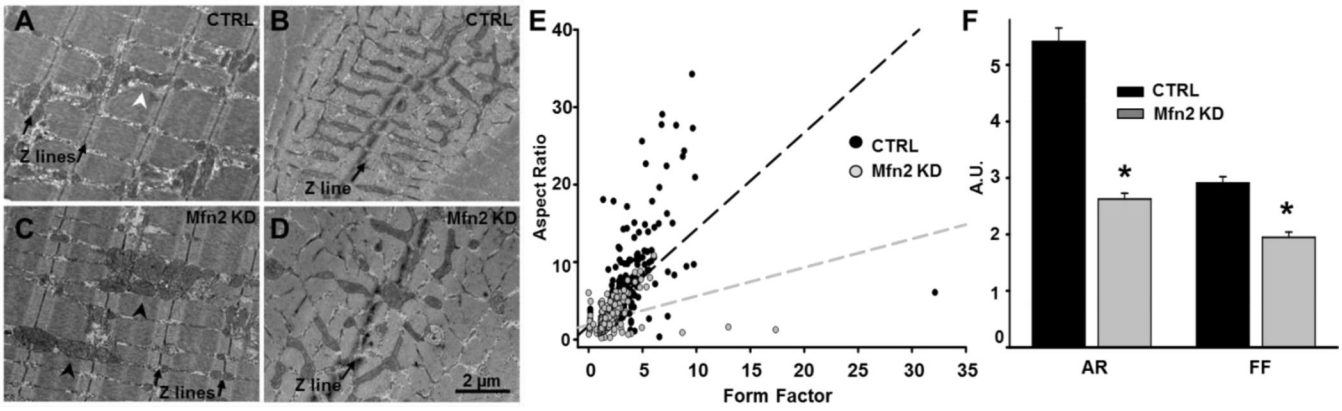

Figure 2.

EM analysis of mitochondrial morphology and intracellular localization. A-D. Representative electron micrographs from CTRL and Mfn2 KD muscles. Longitudinal (A) and cross-section (B) images of CTRL FDB muscle. Mitochondria are primarily positioned within the I band (black arrows) with only rare longitudinal extensions running parallel to the A band (white arrowhead). Longitudinal (C) and cross-section (D) images of Mfn2 KD FDB muscle. Mitochondria are more fragmented, often mis-localized, and more frequently found at the A band (black arrowheads). E. Measures of mitochondrial aspect ratio (AR) and form factor (FF) in CTRL and Mfn2 KD FDB fibers. F. Average values (±SE) of AR and FF in CTRL and Mfn2 KD FDB fibers.

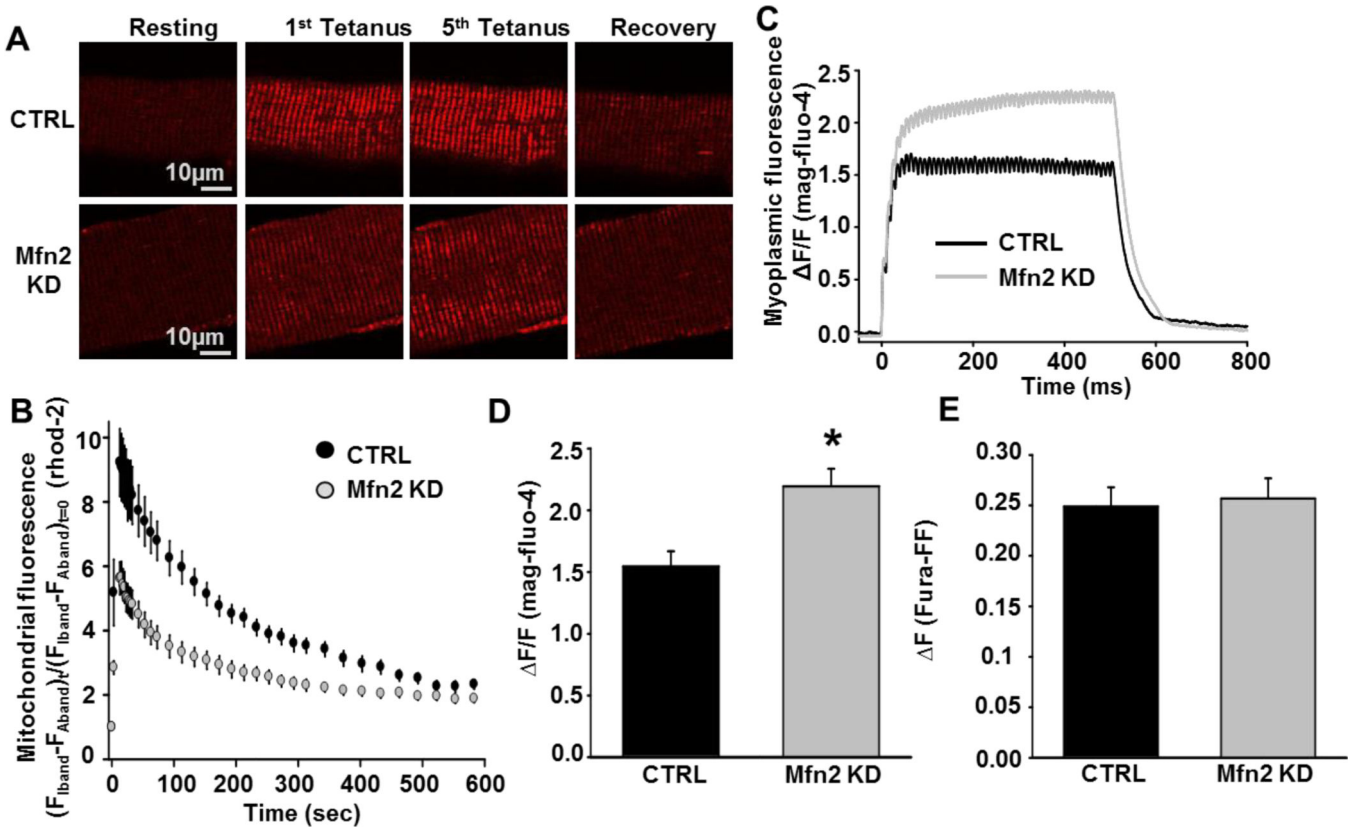

Figure 3.

Measurement of activity-dependent mitochondrial Ca^{2+} uptake in CTRL and Mfn2 KD fibers. A. Representative images of rhod-2 fluorescence in CTRL and Mfn2 KD FDB fibers before, during tetanic stimulation (after 1st and 5th tetani), and 10 minutes after the 5th tetanus. B. Average (±SE) time course of mitochondrial rhod-2 fluorescence in FDB fibers at rest, during 5 successive tetanic stimuli, and for 10 minutes of recovery following the 5th and final tetanus in CTRL (black circles) or Mfn2 KD (grey circles) FDB fibers. C. Representative mag-fluo-4 fluorescence traces in CTRL (black trace) or Mfn2 KD (grey trace) FDB fibers during a single 500ms tetanus. D. Average (±SE) relative myoplasmic mag-fluo-4 fluorescence in CTRL or Mfn2 KD FDB fibers during a single 500ms tetanus. E. Average (±SE) change in fura-FF fluorescence in CTRL or Mfn2 KD FDB fibers following addition of a Ca^{2+} release cocktail consisting of 10 μM ionomycin, 30 μM CPA, and 100 μM EGTA/0 Ca^{2+}.

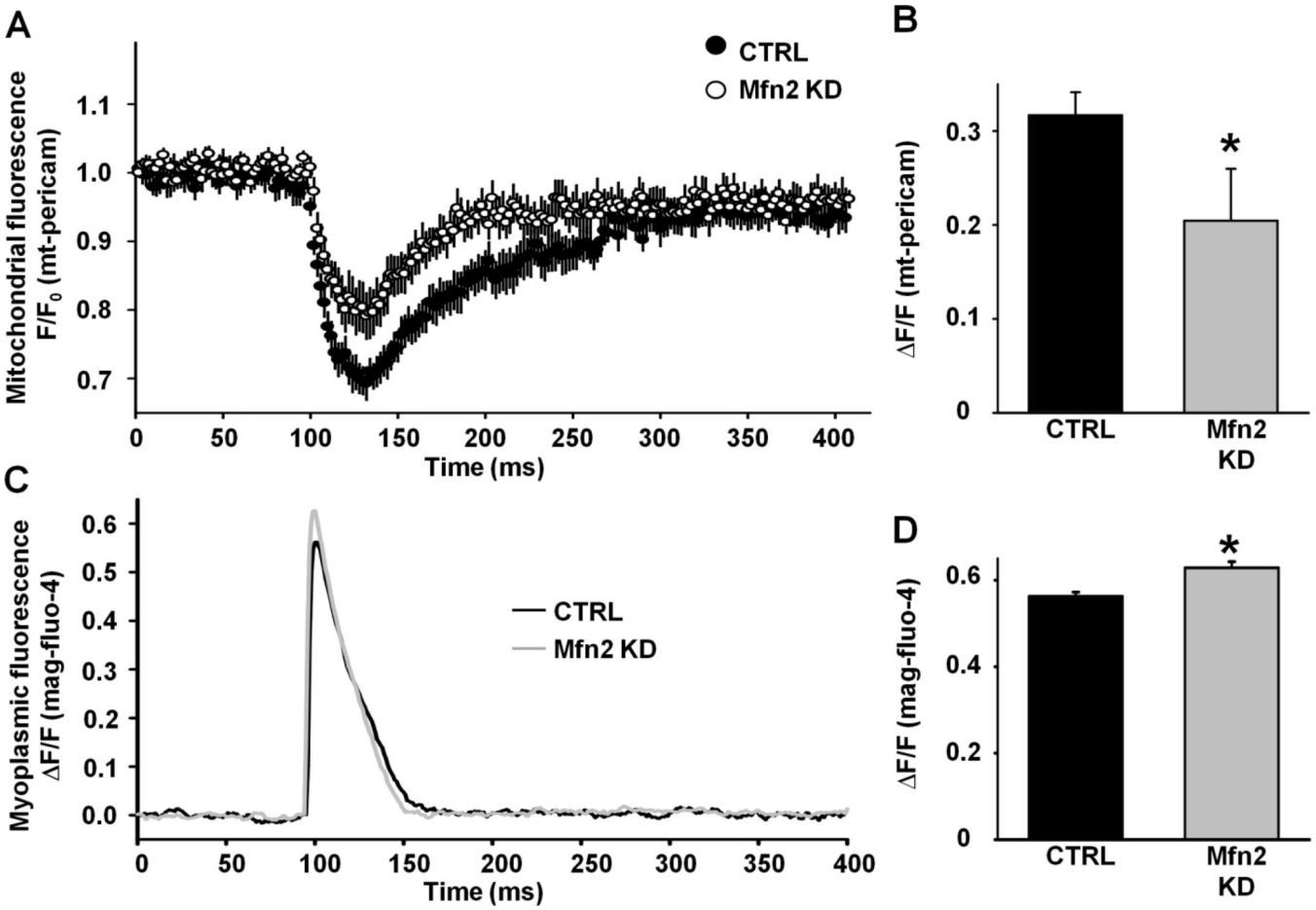

Figure 4.

Measurement of mitochondrial Ca^{2+} uptake during twitch stimulation in mt-pericam expressing CTRL and Mfn2 KD FDB fibers. A. Average (±SE) traces of mt-pericam fluorescence (402 nm excitation/515 nm emission) in CTRL (black circles) and Mfn2 KD (white circles) fibers during twitch stimulation. B. Average (±SE) relative change in mt-pericam fluorescence (ΔF/F) in CTRL and Mfn2 KD FDB fibers during twitch stimulation. C. Representative mag-fluo-4 traces during twitch stimulation of CTRL (black trace) or Mfn2 KD (grey trace) FDB fibers. D. Average (±SE) relative change in myoplasmic mag-fluo-4 fluorescence during twitch stimulation of CTRL or Mfn2 KD FDB fibers.

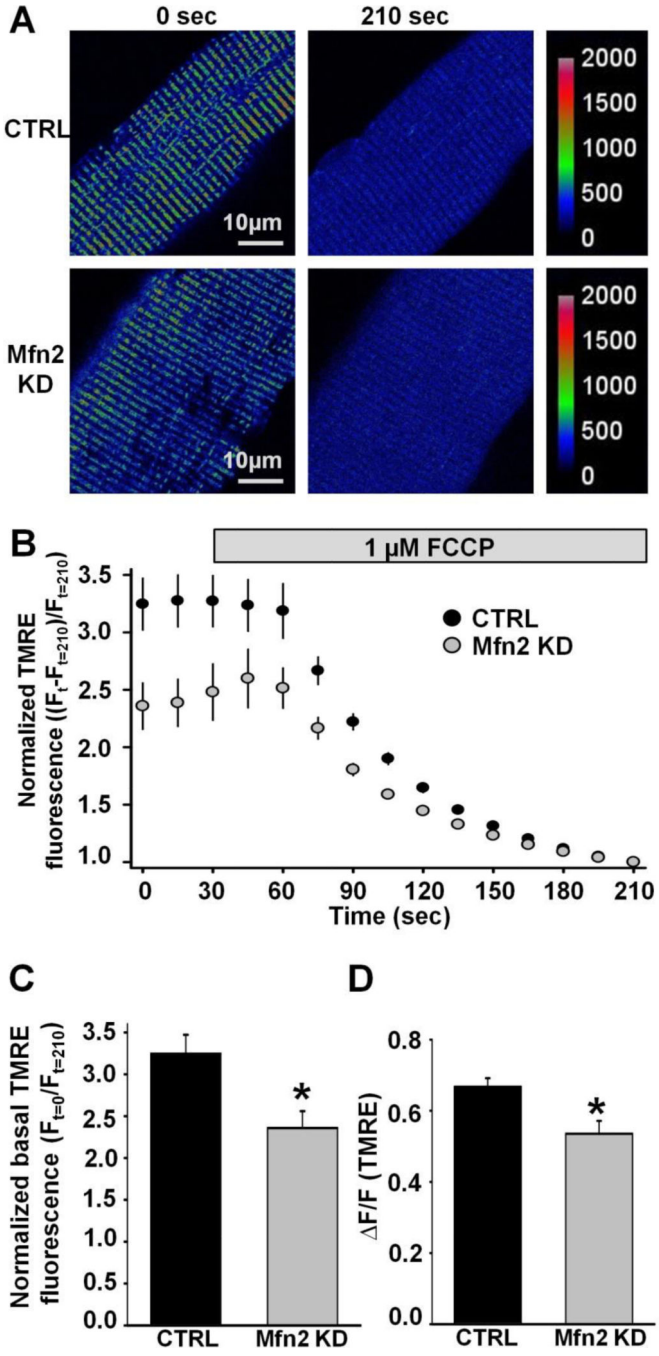

Figure 5.

Measurement of mitochondrial membrane potential in CTRL and Mfn2 KD FDB fibers. A. Representative pseudocolor TMRE confocal images of CTRL and Mfn2 KD FDB fibers before and after application of 1μM FCCP. Scale bars on the right represent relative pseudocolor fluorescence intensities. B. Average (±SE) normalized TMRE fluorescence of CTRL and Mfn2 KD FDB fibers before and during application of 1 μM FCCP (grey bar). C. Average (±SE) normalized baseline TMRE fluorescence in CTRL and Mfn2 KD FDB

fibers. D. Average (±SE) FCCP-sensitive change in TMRE fluorescence in CTRL and Mfn2 KD FDB fibers.

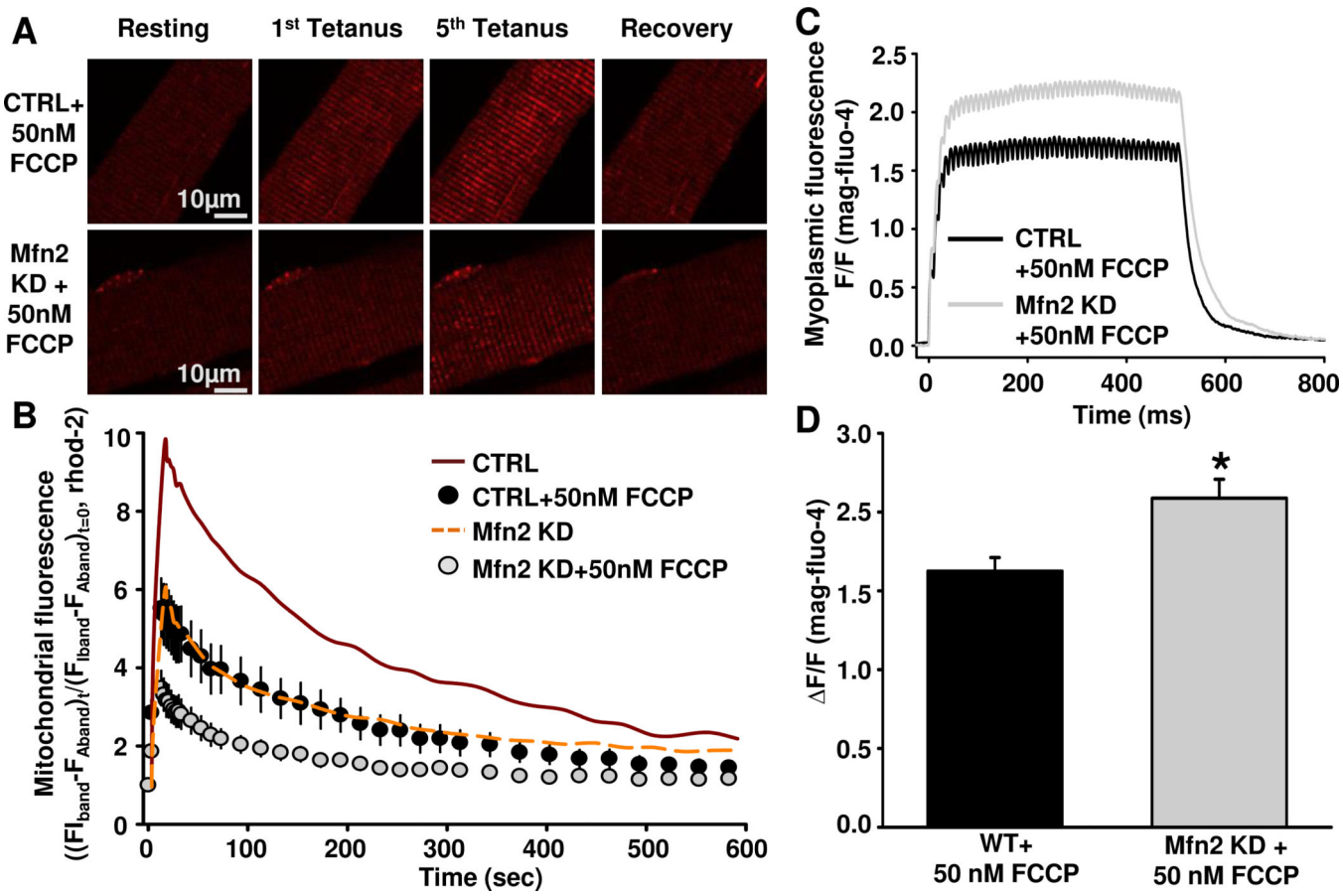

Figure 6.

Measurement of mitochondrial Ca^{2+} uptake in CTRL and Mfn2 KD FDB fibers after 5min incubation in 50nM FCCP. A. Representative images of rhod-2 fluorescence in CTRL FDB fibers + 50nM FCCP or Mfn2 KD fibers + 50nM FCCP before, during tetanic stimulation (after 1st and 5th tetani), and 10 minutes after the 5th tetanus. B. Average (±SE) time course of mitochondrial rhod-2 fluorescence in FDB fibers at rest, during 5 successive tetanic stimuli, and for 10 minutes of recovery following the 5th and final tetanus in CTRL fibers + 50nM FCCP (black circles) or Mfn2 KD fibers + 50nM FCCP (grey circles). CTRL (red solid line) and Mfn2 KD (yellow dashed line) data obtained in the absence of FCCP from Fig. 3B are replotted as line curves again here for comparison C. Representative mag-fluo-4 fluorescence traces in CTRL fibers + 50nM FCCP (black trace) or Mfn2 KD fibers + 50nM FCCP (grey trace) during a single 500ms tetanus. D. Average (±SE) relative myoplasmic mag-fluo-4 fluorescence in CTRL fibers + 50nM FCCP or Mfn2 KD fibers + 50nM FCCP during a single 500ms tetanus.

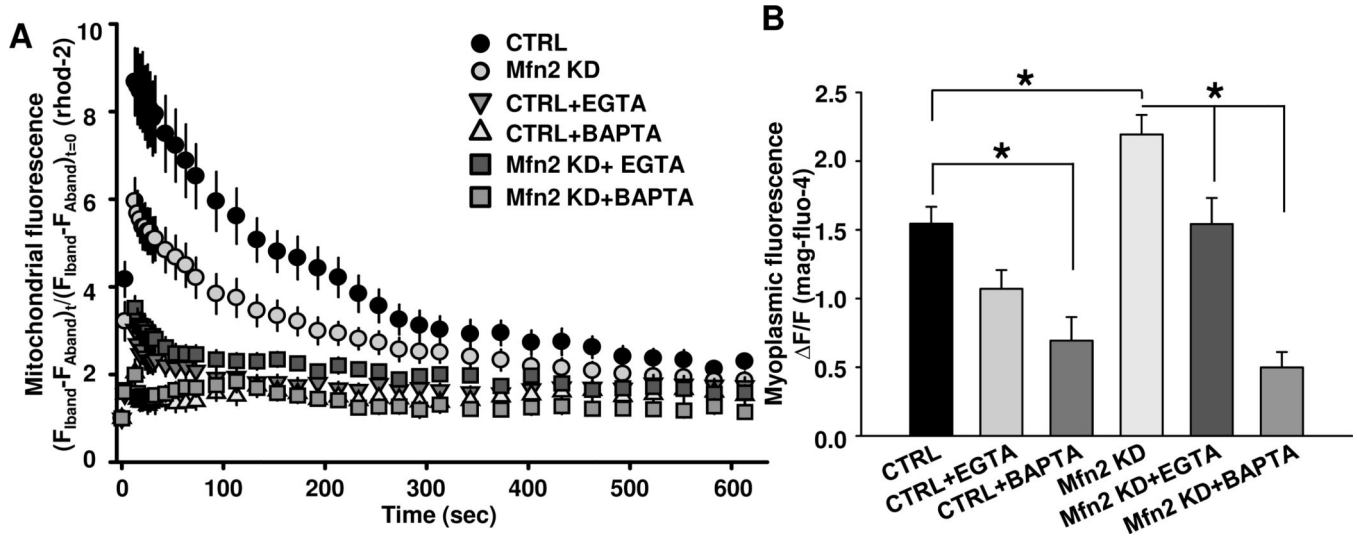

Figure 7.

Measurement of mitochondrial Ca^{2+} uptake in CTRL and Mfn2 KD FDB fibers after incubation with either 20μM EGTA-AM or 20μM BAPTA-AM. A. Average (±SE) time course of mitochondrial rhod-2 fluorescence in FDB fibers at rest, during 5 successive tetanic stimuli, and for 10 minutes of recovery following the 5^{th} and final tetanus in CTRL (black circles) or Mfn2 KD fibers (grey circles). B. Average (±SE) relative myoplasmic mag-fluo-4 fluorescence in CTRL or Mfn2 KD fibers during a single 500ms tetanus.

Table 1

Quantitative analysis of mitochondrial shape and localization.

	A	B	C
	Mitochondrial vol/total vol (%)	**Mitochondrial surface/fiber volume (μm^{-1})**	**Mitochondria at the A band in 100 μm^2 (% of total)**
CTRL	4.24 ± 0.21	7.02 ± 0.26	1.18 ± 0.22 (3.7%)
Mfn2 KD	4.84 ± 0.28	5.17 ± 0.17*	2.08 ± 0.48 (6.4%)*

Values in columns A and B are means ± SE. Values in column C are percent of total mitochondria.

* $p < 0.05$ compared to CTRL.

Table 2

Quantitative analysis of mitochondria-CRUs association and tethers.

	A	B	C
	No. of Mito-CRUs pairs/100 μm^2	**No. of Tethers in 100 Mito/CRUs pairs**	**No. of Tethers in 100 μm^2**
CTRL	51 ± 1	40 ± 1	20 ± 2
Mfn2 KD	21 ± 2*	36 ± 3	7 ± 4*

Values are means ± SE.

* $p < 0.05$ compared to CTRL.